The Astrophysical Journal, 772:49 (9pp), 2013 July 20 doi:10.1088/0004-637X/772/1/49

DO QUIESCENT AND ACTIVE GALAXIES HAVE DIFFERENT $M_{\rm BH}$–σ_* RELATIONS?

Jong-Hak Woo[1,2,7], Andreas Schulze[3], Daeseong Park[1], Wol-Rang Kang[1], Sang Chul Kim[4], and Dominik A. Riechers[5,6]
[1] Astronomy Program, Department of Physics and Astronomy, Seoul National University, 1 Gwanak-ro Gwanak-gu, Seoul, 151-742, Korea; woo@astro.snu.ac.kr
[2] The Observatories of the Carnegie Institution for Science, 813 Santa Barbara St. Pasadena, CA 91101, USA
[3] Kavli Institute for Astronomy and Astrophysics, Peking University, 100871 Beijing, China
[4] Korea Astronomy and Space Science Institute, Daejeon 305-348, Korea
[5] Astronomy Department, Cornell University, 220 Space Science Building, Ithaca, NY 14853, USA
[6] Astronomy Department, California Institute of Technology, MC 249-17, 1200 East California Boulevard, Pasadena, CA 91125, USA
Received 2013 March 24; accepted 2013 May 14; published 2013 July 5

ABSTRACT

To investigate the validity of the assumption that quiescent galaxies and active galaxies follow the same black hole mass ($M_{\rm BH}$)–stellar velocity dispersion (σ_*) relation, as required for the calibration of $M_{\rm BH}$ estimators for broad line active galactic nuclei (AGNs), we determine and compare the $M_{\rm BH}$–σ_* relations, respectively, for quiescent and active galaxies. For the quiescent galaxy sample, composed of 72 dynamical $M_{\rm BH}$ measurements, we update σ_* for 28 galaxies using homogeneous H-band measurements that are corrected for galaxy rotation. For active galaxies, we collect 25 reverberation-mapped AGNs and improve σ_* measurement for two objects. Combining the two samples, we determine the virial factor f, first by scaling the active galaxy sample to the $M_{\rm BH}$–σ_* relation of quiescent galaxies, and second by simultaneously fitting the quiescent and active galaxy samples, as $f = 5.1^{+1.5}_{-1.1}$ and $f = 5.9^{+2.1}_{-1.5}$, respectively. The $M_{\rm BH}$–σ_* relation of active galaxies appears to be shallower than that of quiescent galaxies. However, the discrepancy is caused by a difference in the accessible $M_{\rm BH}$ distribution at given σ_*, primarily due to the difficulty of measuring reliable stellar velocity dispersion for the host galaxies of luminous AGNs. Accounting for the selection effects, we find that active and quiescent galaxies are consistent with following intrinsically the same $M_{\rm BH}$–σ_* relation.

Key words: galaxies: bulges – galaxies: kinematics and dynamics – infrared: galaxies – techniques: spectroscopic

Online-only material: color figures

1. INTRODUCTION

Supermassive black holes (BHs) and their host galaxies appear to coevolve as manifested by the present day correlations between BH mass ($M_{\rm BH}$) and galaxy properties, i.e., $M_{\rm BH}$–stellar velocity dispersion (σ_*) relation (Ferrarese & Merritt 2000; Gebhardt et al. 2000a; Gültekin et al. 2009; McConnell & Ma 2013). These relations are established based on $M_{\rm BH}$ measurements from spatially resolved kinematics of stars (e.g., van der Marel et al. 1998; Gebhardt et al. 2000a), gas (e.g., Ferrarese, Ford & Jaffe 1996; Marconi et al. 2001) or maser (Herrnstein et al. 2005; Kuo et al. 2011) around BH's sphere of influence. While in the early studies the BH–galaxy relations appeared to be very tight, even consistent with zero intrinsic scatter (Gebhardt et al. 2000a), the increased dynamical range and sample size revealed a larger intrinsic scatter of ∼0.5 dex (Gültekin et al. 2009) and significant outliers from the relation (e.g., Hu 2008; Greene et al. 2010; Kormendy et al. 2011; van den Bosch et al. 2012).

Dynamical $M_{\rm BH}$ measurements based on the spatially resolved kinematics are challenging for broad line active galactic nuclei (AGNs) due to the presence of a bright nuclear point source. Instead, an alternative method to measure $M_{\rm BH}$, namely reverberation mapping, has been adopted for broad line AGNs (e.g., Peterson 1993). By employing the variability of AGN, this method measures the time delay between continuum and broad line variability, corresponding to the broad line region (BLR) size ($R_{\rm BLR}$). The black hole mass is then derived via the virial relation $M_{\rm BH} = f\Delta V^2 R_{\rm BLR}/G$, where G is the gravitational constant. The broad line cloud velocity ΔV is measured from the broad line width, and f is a scale factor that depends on the geometry and kinematics of the BLR gas, which is poorly known for individual objects (cf. Brewer et al. 2011; Pancoast et al. 2012). Thus, broad line AGNs are the only available probes to determine $M_{\rm BH}$ out to cosmological distances and test for evolution of the BH–galaxy correlations (e.g., Peng et al. 2006; Woo et al. 2006, 2008; Merloni et al. 2010; Decarli et al. 2010; Cisternas et al. 2011).

Before using AGNs to measure possible redshift evolution in the $M_{\rm BH}$–σ_* relationship, it is necessary to verify whether AGNs follow the same $M_{\rm BH}$–σ_* relationship as quiescent galaxies in the local universe. To first order this seems to be the case, as indicated by early studies of small samples (Gebhardt et al. 2000b; Ferrarese et al. 2001; Nelson et al. 2004). Motivated by these results, Onken et al. (2004) *assumed* that broad line AGNs obey the same $M_{\rm BH}$–σ_* relationship as quiescent galaxies and then empirically determine the unknown factor $f = 5.5 \pm 1.8$ by normalizing the reverberation AGNs to the $M_{\rm BH}$–σ_* relation of quiescent galaxies. Using a significantly increased sample size and dynamical range, Woo et al. (2010) redetermined the scale factor $f = 5.2 \pm 1.2$, and directly fitted the $M_{\rm BH}$–σ_* relation for reverberation-mapped AGN, finding a slope $\beta = 3.55 \pm 0.6$ in the $M_{\rm BH}$–σ_* relation,

$$\log(M_{\rm BH}/M_\odot) = \alpha + \beta \log(\sigma_*/200\ {\rm km\ s^{-1}}), \quad (1)$$

which was shallower than the slope $\beta = 4.24 \pm 0.41$ for quiescent galaxies reported by Gültekin et al. (2009), but consistent within the uncertainties. By adding new $M_{\rm BH}$ measurements of most massive BHs, McConnell & Ma (2013) recently presented an updated $M_{\rm BH}$–σ_* relation for quiescent galaxies, with a significantly steeper slope of $\beta = 5.64 \pm 0.32$.

[7] TJ Park Science Fellow.

Therefore, the slopes of $M_{\rm BH}$–σ_* relation between quiescent and active galaxies are now only consistent with each other on the 2σ level. The observed deviation can be either caused by a pure statistical effect or sample selection, or it may point to a real physical difference of BH–galaxy coevolution between active and predominantly quiescent galaxies. Thus, differentiating between these possibilities will shed light on the coevolution process. Furthermore, since the assumption of similar $M_{\rm BH}$–σ_* relations for quiescent and active galaxies is one of the foundations of the virial $M_{\rm BH}$ estimators, it is required to reinvestigate and compare the $M_{\rm BH}$–σ_* relations of quiescent and active galaxies.

In this paper, we provide updated results on the $M_{\rm BH}$–σ_* relations for quiescent and active galaxies. The quiescent galaxy sample is mainly based on McConnell & Ma (2013), but we added improved and homogeneous near-IR σ_* measurements for a large fraction of the sample from Kang et al. (2013, hereafter K13). The active galaxy sample is based on the reverberation-mapped AGNs from Woo et al. (2010), with the addition of Mrk 50 and updated $M_{\rm BH}$ and new σ_* measurements for part of the sample. Near-IR spectroscopic observations are presented in Section 2, while stellar velocity dispersion measurements are discussed in Section 3. We present and discuss our results on the $M_{\rm BH}$–σ_* relations for quiescent and for active galaxies in Section 4 and investigate whether quiescent and active galaxies have consistent $M_{\rm BH}$–σ_* relations. Conclusions are presented in Section 5.

2. OBSERVATIONS AND DATA REDUCTION

To uniformly measure and improve σ_* using near-IR spectroscopy, we observed 28 quiescent galaxies and 3 reverberation-mapped AGNs. Observation, data reduction, and analysis are presented in detail in K13. Here, we briefly describe observations for three AGNs, which have $M_{\rm BH}$ determined from reverberation mapping results, namely NGC 3227, Akn 120 and 3C 390.3. The stellar velocity dispersions of their host galaxies have been measured previously in the optical, using the Ca II triplet line (Nelson et al. 2004; Onken et al. 2004). For broad line AGNs, σ_* measurements of the host galaxies become increasingly difficult with increasing nuclear-to-host flux ratio due to dilution, in particular in the optical. Measurements in the near-IR have the advantage of an improved nuclear-to-host contrast.

The previous σ_* measurements of Akn 120 and 3C 390.3 were based on low signal-to-noise optical spectra, and hence our near-IR observations could potentially provide a significant improvement on the σ_* measurement. The σ_* of NGC 3227 was measured using a fairly good optical spectrum, but we provide here spatially resolved spectroscopy and are therefore able to correct for the galaxy's rotation component (see below).

Observations were performed with the Triplespec at the Palomar Hale 5 m telescope (Wilson et al. 2004). Triplespec is a near-IR spectrograph with simultaneous coverage from 1.0 μm to 2.4 μm at a spectral resolution of $R = 2500$–2700. We used a long-slit with $1'' \times 30''$, placed along the galaxy's major axis. We performed an ABBA dither pattern along the slit to improve the sky subtraction. For each observing night we observed several A0V stars as telluric standards. We also observed stars of different spectral types as template stars for the σ_* measurement (see K13 for details).

We carried out standard data reduction tasks using IRAF scripts, including bias subtraction, flat-fielding, wavelength calibration and extraction of one-dimensional spectra. For Akn 120 and 3C 390.3 we extracted the spectra within the largest possible aperture ($\pm 7''$) to increase the signal-to-noise. For NGC 3227 we extracted spectra from 13 small extraction windows of the same size along the galaxy's major axis, in order to obtain spatially resolved σ_*. We also extracted spectra from apertures of increasing size to test for the effect of aperture size on our σ_* measurement.

We corrected the spectra for telluric lines, following the method given in K13. Several A0V stars were used to generate a telluric template for each observing night. Averaging over several stars removes small variations between individual stars. The mean telluric template for each night was than used to subtract the telluric lines from the spectra.

3. STELLAR VELOCITY DISPERSIONS

We measured σ_* in the H band, covering several CO lines, Mg I, and Si I simultaneously by directly fitting the observed spectra in pixel space to stellar templates, which were broadened by a Gaussian velocity ranging from 50 to 350 km s^{-1}. The χ^2 minimization was performed using the Gauss–Hermite Pixel Fitting software (van der Marel 1994; Woo et al. 2005), after masking out AGN emission (i.e., Fe II at 1.65 μm), bad pixels, and sky subtraction residuals. We matched the continuum shapes of the broadened templates and the galaxy spectra by fitting low-order polynomials (order 2–4).

To account for template mismatch, we measured σ_* using various M-type template stars (M0 III, M1 III, M2 III, M3 III) since these spectral types provide a consistent match to the observed galaxy spectra in the H-band. We have also used several K giant stars, but found a worse agreement with the observed galaxy spectra. Thus, we have excluded them in the further analysis (see K13 for details). The final σ_* measurements are given by the mean of the measured values from each M-type template, while the quoted uncertainties are determined by adding the standard deviation of the measurements from each template to the mean measurement error in quadrature.

In Figure 1 we present the normalized spectra of the 3 AGNs (black line) along with the best-fit template (red line). A good fit was obtained for NGC 3227 and Akn 120, while the σ_* of 3C 390.3 was not reliably determined since the fits was relatively poor. Thus, we discard the H-band σ_* measurement of 3C 390.3 and use the previous optical measurement from the literature in the further analysis, although our best fit H-band σ_* measurement is in close agreement with the optical measurement. Compared to the previous σ_* measurements from optical spectra, our H-band measurements are slightly smaller (see Table 1). Given the small sample size, however, we cannot conclude whether there is a systematic difference between optical and near-IR measurements. Note that by using a much larger sample of quiescent galaxies we found that velocity dispersions measured in the optical and near-IR are in good agreement in our companion study (K13).

3.1. Rotation and Aperture Effect for NGC 3227

In the case of NGC 3227, we obtained spatially resolved spectra to measure velocity and velocity dispersion along the major axis of the host galaxy. The importance of obtaining spatially resolved spectra rather than single-aperture spectrum for a precise σ_* measurement has been pointed out by previous studies (e.g., Bennert et al. 2011; Harris et al. 2012). In particular, K13 demonstrated that the velocity dispersion can be overestimated by up to $\sim$20% if a single-aperture spectrum is used without correcting for the rotational broadening.

Table 1
Sample and Observations

Name	Obs. Date	R.A.	Decl.	EXPT (s)	S/N	Dist. (Mpc)	Spatial Scale (kpc/1″)	R_e (kpc)	Ref.	$\sigma_{\rm opt}$ (km s^{-1})	Ref.	$\sigma_{\rm IR}$ (km s^{-1})
(1)	(2)	(3)	(4)	(5)	(6)	(7)	(8)	(9)	(10)	(11)	(12)	(13)
Akn 120	2010-01-01	05 16 11.48	−00 09 00.6	3,600	428	141.6	0.68	...	...	221 ± 17	2	192 ± 8
NGC 3227	2010-01-01	10 23 30.58	+19 51 54.2	600	230	17.0	0.08	0.27	1	136 ± 4	2	92 ± 6
3C 390.3	2009-05-22	18 42 08.99	+79 46 17.1	3,200	520	247.3	1.17	...	...	273 ± 16	2	267 ± 14

Notes. Column 1: galaxy name; Column 2: observation date; Column 3: right ascension (J2000); Column 4: declination (J2000); Column 5: total exposure time; Column 6: signal-to-noise ratio per pixel in the extracted spectrum; Column 7: distance; Column 8: spatial scale; Columns 9–10: effective radius and reference; Columns 11–12: the optical stellar velocity dispersion and reference; Column 13: the near-IR stellar velocity dispersion.
References. (1) Davies et al. 2006; (2) Nelson et al. 2004.

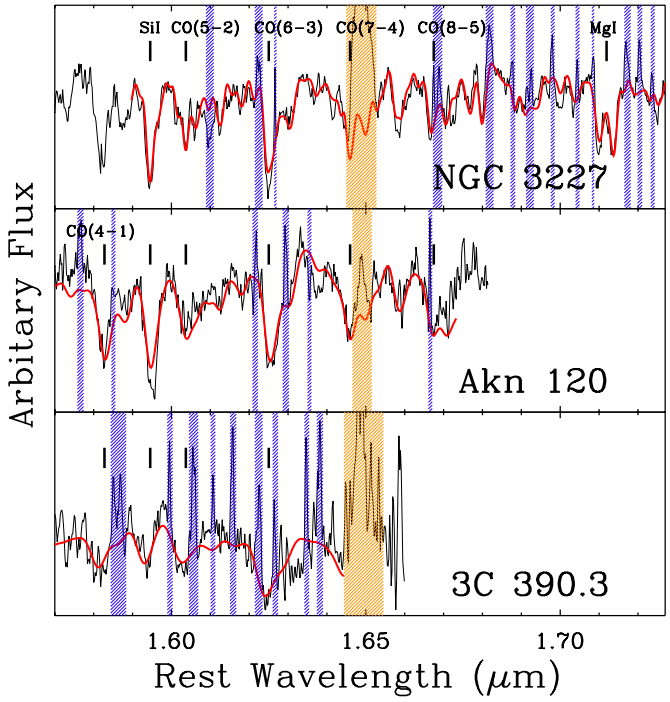

Figure 1. Normalized *H*-band spectra of three active galaxies (black line) overplotted with the best-fit model (red line). Sky emission residuals (blue shade) and the AGN Fe II line (yellow shade) are masked out before fitting.
(A color version of this figure is available in the online journal.)

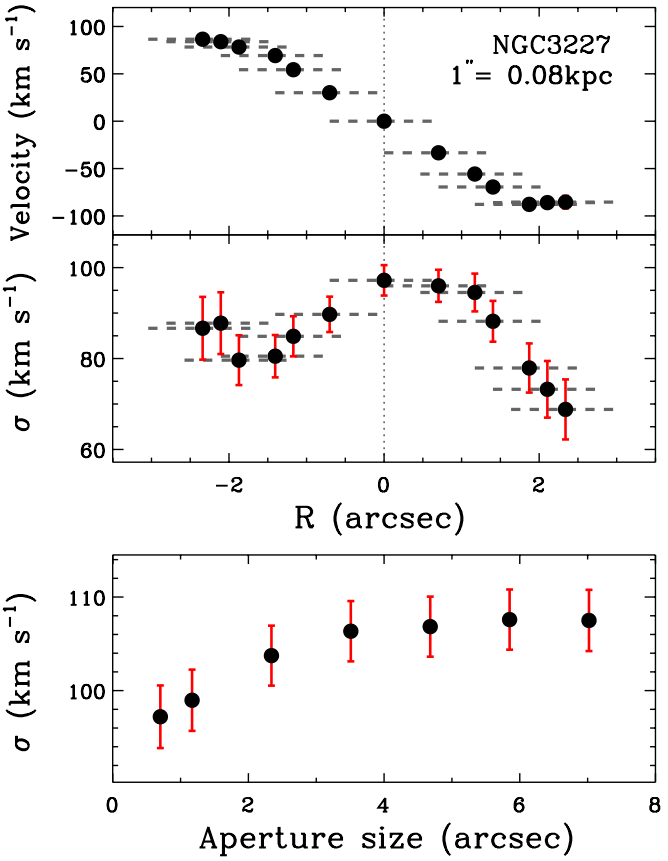

Figure 2. Velocity (top panel) and velocity dispersion profiles (middle panel) of NGC 3227. The bottom panel illustrates the dependence of the measured σ_* on the extraction aperture size.
(A color version of this figure is available in the online journal.)

Figure 2 presents the spatially resolved velocities and velocity dispersions measured along the major axis of NGC 3227. A clear rotation component is present with a maximum projected velocity of ∼100 km s^{-1}. Thus, the rotational broadening would lead to an increase of stellar velocity dispersion if a spectrum extracted from a large aperture is used. To illustrate this, we measured σ_* from a series of spectra extracted from various aperture sizes (Figure 2 lower panel). As expected, the measured σ_* increases with increasing aperture size due to the contribution of the rotation component. The measured σ_* flattens after peaking around $R_{\rm e}$, as the rotation curve flattens at ∼2" and the radial profile of the intrinsic σ_* decreases outward. We corrected for the rotation effect by computing the luminosity-weighted σ_* within the effective radius,

$$\sigma_* = \frac{\int_{-R_e}^{R_e} \sigma_*(r)\, I(r)\, dr}{\int_{-R}^{R} I(r)\, dr} \quad (2)$$

where $I(r)$ is the surface brightness profile of the galaxy measured from the spectral image and R_e is the effective radius. We find the luminosity-weighted $\sigma_* = 92 \pm 6$ km s^{-1}, while the uncorrected value based on a single-aperture spectrum is 106 ± 7 km s^{-1}, i.e., we overestimate σ_* by 15% if we do not correct for the rotation component. Note that the rotation effect on σ_* measurements will vary for individual galaxies since it depends on the inclination angle of the rotating disk to the line-of-sight and the maximum rotation velocities (see K13 for details).

4. THE $M_{\rm BH}$–σ_* RELATION

4.1. The M_{BH}–σ_* Relation of Quiescent Galaxies

Much effort has been invested to improve the $M_{\rm BH}$–σ_* relation since its discovery by increasing the sample size and

Table 2
Updated M_{BH} and σ_* Measurements for Quiescent Galaxies

Name	M_{BH} ($10^8\ M_\odot$)	σ_* (km s^{-1})
(1)	(2)	(3)
N221	$0.026^{+0.005}_{-0.005}$	65 ± 2
N821	$1.7^{+0.7}_{-0.7}$	191 ± 8
N1023	$0.40^{+0.04}_{-0.04}$	205 ± 6
N2787	$0.41^{+0.04}_{-0.05}$	170 ± 4
N3031	$0.80^{+0.20}_{-0.11}$	165 ± 4
N3115	$8.9^{+5.1}_{-2.7}$	236 ± 9
N3227	$0.15^{+0.05}_{-0.08}$	92 ± 6
N3245	$2.1^{+0.5}_{-0.6}$	192 ± 6
N3377	$1.8^{+0.9}_{-0.9}$	127 ± 3
N3379	$4.2^{+1.0}_{-1.1}$	205 ± 6
N3384	$0.11^{+0.05}_{-0.05}$	129 ± 4
N3607	$1.4^{+0.4}_{-0.5}$	198 ± 7
N3608	$4.7^{+1.0}_{-1.0}$	193 ± 5
N4258	$0.367^{+0.001}_{-0.001}$	109 ± 4
N4261	$5.3^{+1.1}_{-1.1}$	304 ± 8
N4291	$9.8^{+3.1}_{-3.1}$	245 ± 7
N4342	$4.6^{+2.6}_{-1.5}$	199 ± 8
N4374	$9.2^{+1.0}_{-0.8}$	292 ± 9
N4459	$0.70^{+0.13}_{-0.14}$	156 ± 7
N4473	$0.89^{+0.45}_{-0.44}$	173 ± 5
N4486	62^{+3}_{-4}	327 ± 11
N4564	$0.88^{+0.24}_{-0.24}$	166 ± 6
N4596	$0.84^{+0.36}_{-0.25}$	136 ± 5
N4649	47^{+11}_{-10}	311 ± 12
N4697	$2.0^{+0.2}_{-0.2}$	153 ± 4
N5845	$4.9^{+1.5}_{-1.6}$	223 ± 5
N6251	$6.0^{+2.0}_{-2.0}$	296 ± 13
N7052	$4.0^{+2.8}_{-1.6}$	334 ± 15

Notes. Column 1: galaxy name; Column 2: M_{BH} taken from McConnell & Ma (2013; see references therein); Column 3: rotation-corrected stellar velocity dispersions taken from K13.

the dynamical range (e.g., Gültekin et al. 2009; Nowak et al. 2010; McConnell et al. 2012), and by improving the previous M_{BH} measurements (e.g., van den Bosch & de Zeeuw 2010; Shen & Gebhardt 2010; Schulze & Gebhardt 2011; Gebhardt et al. 2011). In contrast, σ_* measurements for many objects are still often based on rather inhomogeneous literature data. To overcome this limitation, we homogeneously measured σ_* based on the uniformly taken H-band spectra for a sample of 28 quiescent galaxies, as presented by K13, which is almost half the size of the most recent compilation of M_{BH} measurements (McConnell & Ma 2013). In particular, these σ_* measurements were corrected for the effect of rotation based on the spatially resolved measurements using Equation (2), as similarly performed for NGC 3227 in Section 3.1.

Incorporating these new σ_* measurements from our companion work (K13), we here update the M_{BH}–σ_* relationship for quiescent galaxies. The sample is based on the catalog of 72 galaxies presented by McConnell & Ma (2013), of which we updated σ_* for 28 objects, taken from K13. In Table 2, we list M_{BH} and σ_* for the updated galaxies. To fit the M_{BH}–σ_* relationship we assumed the common single-index power law as

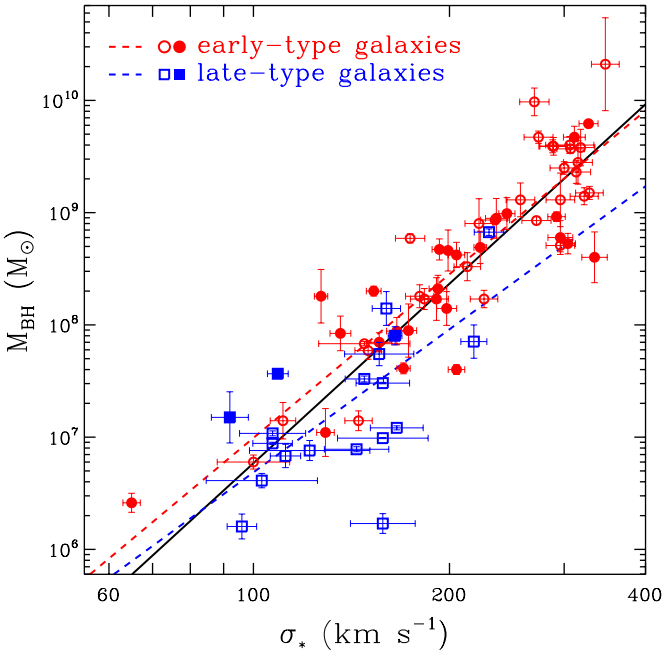

Figure 3. M_{BH}–σ_* relation of quiescent galaxies for the full sample (black line), early-type galaxies (red circles, red dashed line), and late-type galaxies (blue squares, blue dashed line). The rotation-corrected H-band σ_* measurements are denoted with filled symbols while the rotation-included σ_* values from the literature are marked with open symbols.
(A color version of this figure is available in the online journal.)

expressed in Equation (1), and used two different fitting methods: the modified FITEXY method, accounting for intrinsic scatter in the fit (Tremaine et al. 2002), and the maximum likelihood method (Gültekin et al. 2009; Schulze & Gebhardt 2011; see Park et al. 2012a for more details on the comparison of these fitting techniques). As we found consistent results between both methods, we only provide the results from the FITEXY method. For this method, we minimize

$$\chi^2 = \sum_{i=1}^{N} \frac{(\mu_i - \alpha - \beta s_i)^2}{\sigma_{\mu,i}^2 + \beta^2 \sigma_{s,i}^2 + \epsilon_0^2}\ , \quad (3)$$

with $\mu = \log(M_{BH}/M_\odot)$, $s = \log(\sigma_*/200\,\mathrm{km\,s^{-1}})$, measurement uncertainties σ_μ and σ_s in both variables, and intrinsic scatter ϵ_0. We obtain the best-fit result for the full sample and for completeness, and we also fit the M_{BH}–σ_* relation for each subsample, e.g., classical bulges, pseudo-bulges, core galaxies, and power-law galaxies, using classifications from the literature (Kormendy et al. 2011; Greene et al. 2010; Gültekin et al. 2009; McConnell & Ma 2013). The best fit results are listed in Table 3, showing that the slopes of the M_{BH}–σ_* relation for these subsample are more or less similar except pseudo-bulge galaxies. The much shallower slope of the M_{BH}–σ_* relation of pseudo-bulge galaxies is qualitatively consistent with the previous claims that pseudo-bulge galaxies do not follow the same M_{BH}–σ_* relation as classical bulges (Hu 2008; Graham 2008; Gadotti & Kauffmann 2009; Greene et al. 2010; Kormendy et al. 2011).

For the full sample, the slope ($\beta = 5.31 \pm 0.33$) is slightly lower than that of McConnell & Ma (2013) but consistent within the uncertainties (see Figure 3). The difference is partly due to the method of calculating effective velocity dispersions. While we determined the effective velocity dispersion by calculating luminosity-weighted velocity dispersion using Equation (2), McConnell & Ma (2013; see also Gültekin et al. 2009)

Table 3
Fits to the M_{BH}–σ_* Relationship

Sample	N_{gal}	Rotation-corrected σ_*			Rotation-included σ_*		
		α	β	ϵ_0	α	β	ϵ_0
Full	72	8.37 ± 0.05	5.31 ± 0.33	0.41 ± 0.05	8.33 ± 0.05	5.48 ± 0.32	0.39 ± 0.05
Early-type	53	8.45 ± 0.05	4.84 ± 0.36	0.35 ± 0.04	8.40 ± 0.06	5.04 ± 0.36	0.35 ± 0.04
Late-type	19	7.96 ± 0.26	4.23 ± 1.26	0.48 ± 0.10	8.03 ± 0.26	4.75 ± 1.21	0.45 ± 0.11
Classical bulges	54	8.49 ± 0.05	4.57 ± 0.33	0.33 ± 0.04	8.45 ± 0.05	4.76 ± 0.33	0.33 ± 0.04
Pseudo-bulges	17	7.66 ± 0.25	3.28 ± 1.11	0.35 ± 0.12	7.68 ± 0.29	3.56 ± 1.64	0.33 ± 0.11
Core	28	8.55 ± 0.09	4.67 ± 0.69	0.34 ± 0.06	8.55 ± 0.10	4.66 ± 0.74	0.35 ± 0.06
Power-law	18	8.30 ± 0.09	4.07 ± 0.66	0.37 ± 0.07	8.22 ± 0.08	4.31 ± 0.61	0.34 ± 0.07
Barred	11	7.75 ± 0.14	2.21 ± 0.82	0.32 ± 0.08	7.76 ± 0.16	2.40 ± 0.88	0.31 ± 0.08
Non-barred	61	8.39 ± 0.05	5.44 ± 0.38	0.39 ± 0.06	8.35 ± 0.05	5.59 ± 0.37	0.37 ± 0.05
Reverberation-mapped AGN	25	7.31 ± 0.15	3.46 ± 0.61	0.41 ± 0.05			
Quiescent + AGN	97	8.36 ± 0.05	4.93 ± 0.28	0.43 ± 0.04			

Notes. Rotation-corrected velocity dispersions are available only for 28 objects in the quiescent galaxy sample from K13 (see Table 2) and for 1 object (NGC 3227) in the active galaxy sample from this study.

added rotation velocity to velocity dispersion in quadrature in calculating effective velocity dispersion within the effective radius, as

$$\sigma_*^2 = \frac{\int_{-R_e}^{R_e} (\sigma_*(r)^2 + V(r)^2)\, I(r)\, dr}{\int_{-R_e}^{R_e} I(r)\, dr} \quad (4)$$

where $I(r)$ is the surface brightness of the galaxy and R_e is the effective radius. Nevertheless, the change of the final adopted σ_* due to the inclusion or exclusion of rotation velocity is not significant for early-type galaxies because rotation velocity is relatively small and the central velocity dispersion is dominant in the luminosity-weight. In contrast, the rotation effect is potentially important for late-type galaxies, whose rotation velocity is comparable to velocity dispersion. Note that we combined the rotation-corrected velocity dispersion for 28 galaxies based on our previous work (K13) with the rotation-included velocity dispersion for the other 44 galaxies, for which rotation-corrected velocity dispersions are not available from McConnell & Ma (2013). To quantify the effect of rotation, we used rotation-included σ_* using Equation (4) for the full sample, and fit the M_{BH}–σ_* relation for various subsamples as listed in Table 3. As the effective velocity dispersion increases due to the inclusion of rotation velocity, the slope of the M_{BH}–σ_* relation slightly steepens for each subsample.

We find that late-type galaxies have a slightly shallower slope than early-type galaxies, while McConnell & Ma (2013) claimed a consistent slope of the M_{BH}–σ_* relation between early-type and late-type subsamples. As the effect of rotation is potentially much stronger in late-type galaxies than in early-type galaxies, it should be further tested whether early- and late-type galaxies have a consistent slope of the M_{BH}–σ_* relation, using a larger sample of late-type galaxies with/without rotation correction. Note that rotation-corrected σ_* are only available for three late-type galaxies in the sample. Applying such a correction to the remaining galaxies will mainly reduce σ_* for late-type and low σ_* galaxies, thus presumably flattening the slope of the M_{BH}–σ_* relationship.

In order to understand the origin of the M_{BH}–σ_* relation, the slope of the relation provides insight in the physical feedback process. For example, theoretical models propose a slope of 4 for feedback by momentum-driven winds (Fabian 1999; King 2003; Murray et al. 2005), while energy-driven winds lead to a slope of 5 (Silk & Rees 1998). For the full sample, we find a slope ∼5, supporting energy-driven winds. However, note that the rotation effect has not been corrected for most of low-mass and late-type galaxies. Thus, it is possible that the slope may be overestimated if σ_* of these late-type galaxies at low-mass scale were overestimated due to the rotation effect. We caution that uncertainties in the slope are still large and selection effects will probably lead to a steeper slope in the M_{BH}–σ_* relation (Gültekin et al. 2009; Schulze & Wisotzki 2011; Morabito & Dai 2012). We also note that the slope can significantly change depending on the fitting direction (forward versus inverse regression; see Section 4.4 for more discussion; Schulze & Wisotzki 2011; Graham et al. 2011; Park et al. 2012a).

4.2. The M_{BH}–σ_* Relation of Active Galaxies

We present the M_{BH}–σ_* relation for reverberation-mapped AGNs using the sample compiled by Woo et al. (2010) with the following updates: (1) improved σ_* measurements for two AGNs (NGC 3227 and Akn 120), as presented in Section 3, (2) improved virial products for nine AGNs from the Lick AGN Monitoring Project (Park et al. 2012b), (3) the addition of Mrk 50 (Barth et al. 2011). It would be desirable to separate the AGN sample into subsamples, i.e., early/late-type and classical/pseudo bulges, as we did for the quiescent galaxy sample. However, obtaining a reliable classification for the host galaxies of broad line AGNs is hampered by the presence of a bright AGN (e.g., Bentz et al. 2009), hence not available for the sample. Thus, we restrict our analysis to the full AGN sample although we note that our AGN sample is biased toward late-type galaxies and a significant fraction is expected to contain pseudo-bulges.

Assuming the same form for the M_{BH}–σ_* relation as for quiescent galaxies, we fit the relation for the AGN sample. Using the virial product in Table 4, we obtain $\alpha = 7.31 \pm 0.15$, $\beta = 3.46 \pm 0.61$ and an intrinsic scatter of $\epsilon_0 = 0.41 \pm 0.05$. The slope is flatter than that of quiescent galaxies, but fully consistent with previous results on the M_{BH}–σ_* relation of active galaxies. For example, Woo et al. (2010) reported a slope of $\beta = 3.55 \pm 0.6$ for their reverberation-mapped AGN sample. In the case of type-1 AGNs without reverberation mapping data, a similar slope, ranging from 3.3 to 3.7 has been reported by various studies (Greene & Ho 2006; Shen et al. 2008; Bennert et al. 2011; Xiao et al. 2011), based on single-epoch M_{BH}

Table 4
Virial Products and σ_* for Reverberation AGN

Name	VP $\sigma^2_{\rm line} R_{\rm BLR}/G$ ($10^6 M_\odot$)	Ref.	σ_* (km s^{-1})	Ref.
(1)	(2)	(3)	(4)	(5)
Akn 120	27.2 ± 3.5	2	192 ± 8	This work
Arp 151	$1.31^{+0.18}_{-0.23}$	3	118 ± 4	7
Mrk 50	6.2 ± 0.9	6	109 ± 14	6
Mrk 79	9.52 ± 2.61	2	130 ± 12	9
Mrk 110	4.57 ± 1.1	2	91 ± 7	10
Mrk 202	$0.55^{+0.32}_{-0.22}$	3	78 ± 3	7
Mrk 279	6.35 ± 1.67	2	197 ± 12	9
Mrk 590	8.64 ± 1.34	2	189 ± 6	9
Mrk 817	$11.3^{+2.7}_{-2.8}$	1	120 ± 15	9
Mrk 1310	0.61 ± 0.20	3	84 ± 5	7
NGC 3227	$1.39^{+0.29}_{-0.31}$	1	92 ± 6	This work
NGC 3516	$5.76^{+0.51}_{-0.76}$	1	181 ± 5	9
NGC 3783	5.42 ± 0.99	2	95 ± 10	11
NGC 4051	$0.31^{+0.10}_{-0.09}$	1	89 ± 3	9
NGC 4151	$8.31^{+1.04}_{-0.85}$	4	97 ± 3	9
NGC 4253	$0.35^{+0.15}_{-0.14}$	3	93 ± 32	7
NGC 4593	1.78 ± 0.38	5	135 ± 6	9
NGC 4748	$0.68^{+0.24}_{-0.30}$	3	105 ± 13	7
NGC 5548	$12.41^{3.06}_{-4.21}$	3	195 ± 13	7
NGC 6814	$3.73^{+1.10}_{-1.11}$	3	95 ± 3	7
NGC 7469	2.21 ± 0.25	2	131 ± 5	9
SBS 1116+583A	$1.08^{+0.52}_{-0.49}$	3	92 ± 4	7
PG 1426+015	236 ± 70	2	217 ± 15	12
3C 120	$10.1^{+5.7}_{-4.1}$	2	162 ± 20	8
3C 390.3	52.2 ± 11.7	2	273 ± 16	9

Notes. Column 1: galaxy name; Column 2: virial product ($M_{\rm BH} = f \times {\rm VP}$); Column 3: reference for $M_{\rm BH}$; Column 4: stellar velocity dispersion; Column 5: reference for σ_*.

References. (1) Denney et al. 2010; (2) Peterson et al. 2004; (3) Park et al. 2012b; (4) Bentz et al. 2006; (5) Denney et al. 2006; (6) Barth et al. 2011; (7) Woo et al. 2010; (8) Nelson & Whittle 1995; (9) Nelson et al. 2004; (10) Ferrarese et al. 2001; (11) Onken et al. 2004; (12) Watson et al. 2008.

estimates and σ_* measurements. Thus, the apparent flattening of the $M_{\rm BH}$–σ_* relation for AGN samples is well established. In Section 4.4, we will address whether this is evidence for an intrinsic difference between active and inactive BHs and their galaxies, or it can be understood by differences in the sample selection.

4.3. The Virial Factor

For type 1 AGNs reverberation mapping provides an alternative method to measure $M_{\rm BH}$. However, apart from a few recent exceptions (Brewer et al. 2011; Pancoast et al. 2012), only the virial product (VP) can be obtained which deviates from the actual $M_{\rm BH}$ by an unknown normalization factor f as expressed in Section 1. This f factor is either determined by assumptions about the geometry of the BLR (e.g., Netzer et al. 1990), or by scaling of the reverberation mapping sample to the $M_{\rm BH}$–σ_* relation of quiescent galaxies (Onken et al. 2004; Woo et al. 2010). A fully spherical BLR corresponds to a virial factor $f = 3$ (e.g., Kaspi et al. 2000), while if the BLR is modeled by a rotating disk, the virial factor is viewing-angle-dependent (e.g., Collin et al. 2006). Scaling the reverberation mapping sample to the quiescent galaxy $M_{\rm BH}$–σ_* relation is an independent approach to determine the average virial factor f. The underlying assumption of this approach is that AGNs obey the same relation as quiescent galaxies.

Based on a sample of 16 reverberation mapping AGNs, Onken et al. (2004) reported a virial factor of $f = 5.5$, adopting the relations from Tremaine et al. (2002) and Ferrarese (2002). Woo et al. (2010) obtained $f = 5.2$ and $f = 5.1$, calibrating an enlarged sample of 24 AGNs to the relations of Gültekin et al. (2009) and Ferrarese & Ford (2005), respectively. Graham et al. (2011) reported a smaller value of $f = 3.8$ by calibrating the AGN sample to the $M_{\rm BH}$–σ_* relation for quiescent galaxies presented in their paper. Recently, Park et al. (2012a) investigated the origin of this discrepancy in the determination of f in the last two studies. They concluded that the difference is mainly due to the sample selection in both studies. Indeed, the $M_{\rm BH}$–σ_* relation reported by Graham et al. (2011) is offset by 0.2 dex compared to our results in Section 4.1. Using the $M_{\rm BH}$–σ_* from McConnell et al. (2011), Park et al. (2012a) obtained $f = 5.1$, in excellent agreement with the results of Woo et al. (2010).

We here provide a new determination of the virial factor, based on the updated reverberation mapping AGN sample presented in Section 4.2, calibrated to the quiescent galaxy sample presented in Section 4.1. We fitted the AGN sample with the FITEXY and maximum likelihood method, but fixed the slope to $\beta = 5.31$, found for the quiescent galaxy sample. As we were using only virial products instead of $M_{\rm BH}$ for the AGN sample, the virial factor f is given by $\log f = \alpha_{\rm quiescent} - \alpha_{\rm AGN}$. Using the FITEXY method, we obtain a virial factor $\log f = 0.71 \pm 0.11$, corresponding to $f = 5.1^{+1.5}_{-1.1}$, and intrinsic scatter $\epsilon_0 = 0.49 \pm 0.05$, consistent with most previous results.

As we have shown above, the slope of the AGN sample is not consistent with the slope found for the quiescent galaxy sample. This may potentially lead to a bias on the determined virial factor. If we hold to the assumption that quiescent and active galaxies follow the same $M_{\rm BH}$–σ_* relation, the most consistent approach is to fit the quiescent galaxy sample and the AGN sample together, determining the $M_{\rm BH}$–σ_* relation and the virial factor jointly. This can be easily achieved by the maximum likelihood method, where we minimize the likelihood $S = -2 \ln \mathcal{L}$. In our case, the likelihood function S is then the sum of the likelihood functions for the quiescent and active galaxies,

$$S = \sum_{i=1}^{N} \left[\frac{(\mu_i - \alpha - \beta s_i)^2}{\epsilon^2_{{\rm tot},i}} + 2 \ln \epsilon_{{\rm tot},i} \right] + \sum_{j=1}^{M} \left[\frac{(\mu_{{\rm VP},j} + \log f - \alpha - \beta s_j)^2}{\epsilon^2_{{\rm tot},j} + \epsilon^2_f} + 2 \ln \sqrt{\epsilon^2_{{\rm tot},j} + \epsilon^2_f} \right], \quad (5)$$

where $\mu_{\rm VP} = \log {\rm VP}$, $\epsilon^2_{\rm tot} = \sigma^2_\mu + \beta^2 \sigma^2_s + \epsilon^2_0$, N is the number of galaxies with dynamical mass measurements and M is the number of AGN with reverberation mapping masses. We simultaneously fit for the zero point α, slope β and intrinsic scatter ϵ_0 of the $M_{\rm BH}$–σ_* relation and for the mean virial factor $\log f$ and its intrinsic scatter ϵ_f. Our best fit results are $\alpha = 8.36 \pm 0.05$, $\beta = 4.78 \pm 0.26$, $\epsilon_0 = 0.42 \pm 0.04$ and $\log f = 0.79 \pm 0.13$, consistent with our previous results. The data do not show evidence for an additional intrinsic scatter in the f value. This may suggest an intrinsic small spread in the virial factor, for example, due to small variation in the viewing angle onto a non-spherical BLR. Another possible explanation

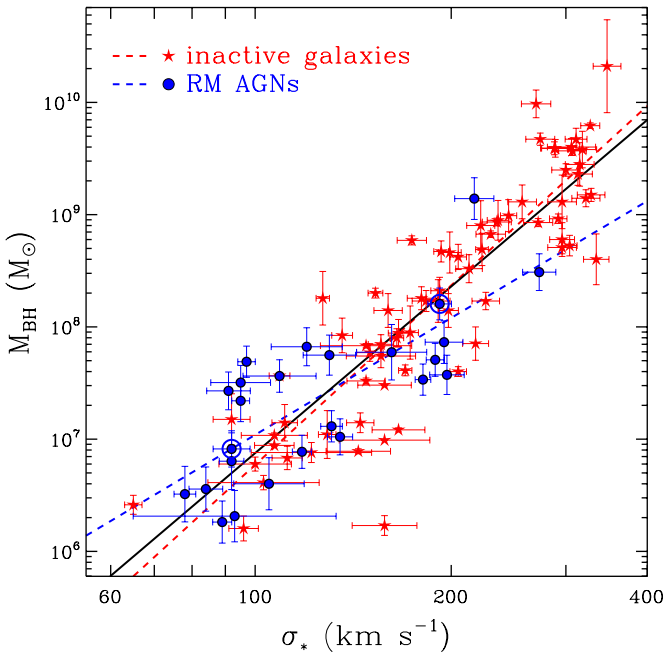

Figure 4. M_{BH}–σ_* relation for active (blue circles) and quiescent galaxies (red stars). The two AGNs with updated σ_* are marked with big blue circles. The red dashed line represents the best fit for quiescent galaxies, as in Figure 3, the blue dashed line shows the relation for the reverberation-mapped AGNs (assuming $f = 5.9^{+2.1}_{-1.5}$ based on the joint fit), and the black solid line shows the best fit to the combined quiescent and active galaxy samples.

(A color version of this figure is available in the online journal.)

for the apparent lack of scatter in f is that measurement uncertainties are under- or overestimated in the quiescent and/or active galaxy samples.

Assuming zero intrinsic scatter in the f value, we can also use a modified version of the FITEXY method to obtain the M_{BH}–σ_* relation and the f factor jointly. Here, we minimize

$$\chi^2 = \sum_{i=1}^{N} \frac{(\mu_i - \alpha - \beta s_i)^2}{\sigma_{\mu,i}^2 + \beta^2 \sigma_{s,i}^2 + \epsilon_0^2} + \sum_{j=1}^{M} \frac{(\mu_{\mathrm{VP},j} + \log f - \alpha - \beta s_j)^2}{\sigma_{\mu,j}^2 + \beta^2 \sigma_{s,j}^2 + \epsilon_0^2}, \quad (6)$$

where we change ϵ_0 such that we obtain a reduced χ^2 of unity. The best fit using this modified FITEXY is $\alpha = 8.36 \pm 0.05$, $\beta = 4.93 \pm 0.28$, $\epsilon_0 = 0.43 \pm 0.04$ and $\log f = 0.77 \pm 0.13$, fully consistent with the results above. This corresponds to a virial factor $f = 5.9^{+2.1}_{-1.5}$.

4.4. Are the M_{BH}–σ_* Relations of Quiescent and Active Galaxies Different?

From a physical perspective it is not clear whether active galaxies should follow exactly the same M_{BH}–σ_* relation as inactive galaxies, as they are in a special evolutionary phase of ongoing BH growth although the BH growth rate may not be very high. To first order, the overlap between the two samples, seen in Figure 4, suggests that active and inactive galaxies do obey the same relation. As discussed above, however, the zero-point of the relation is ensured by design. In contrast, the measured slopes of the two relations appear to be mildly inconsistent with each other, implying that quiescent and active galaxies have different M_{BH}–σ_* relations.

Note that both samples rely on very different methods of estimating M_{BH}, and it is not well tested whether both methods give the same mass measurements. Currently, M_{BH} measurements are available only for two objects (NGC 3227 and NGC 4151) from both dynamical method *and* reverberation mapping techniques, which are in reasonable agreement (Davies et al. 2006; Denney et al. 2010; Onken et al. 2007; Hicks & Malkan 2008; Bentz et al. 2006). However, more such cases are required to draw firm conclusions whether dynamical method and reverberation mapping technique provide consistent results.

How can we then understand the apparent difference in the slope of the M_{BH}–σ_* relation between active and quiescent galaxy samples? It may imply a real physical difference, for example, caused by a different evolutionary stage in the BH growth phase, where active BHs in less massive galaxies are still in the process of growing toward the quiescent M_{BH}–σ_* relation. Alternatively, the apparent difference could be simply due to the sample selection. In fact, galaxies studied with dynamical methods and those studied via reverberation mapping obey different selection criteria. The main observational limitation for dynamical methods is the requirement to approximately spatially resolve the BH's sphere of influence, given by $R_{\mathrm{inf}} = GM_{BH}\sigma_*^{-2}$. This naturally limits the applicability of this method to nearby galaxies, but also excludes a specific subset within this local volume. BHs with smaller spheres of influence are removed from the sample, either implicitly by the target selection or through the ability to detect the BH (Batcheldor 2010; Schulze & Wisotzki 2011).

Contrary, reverberation mapping does not depend on spatial resolution. However, it requires the presence of broad AGN emission lines and sufficient AGN variability to first classify the galaxy as harboring an AGN and secondly measure a secure time lag. This introduces several selection effects to the AGN M_{BH}–σ_* sample, including an active fraction bias and a luminosity bias as discussed by Schulze & Wisotzki (2011). An active fraction bias is introduced if lower mass BHs have a higher probability to be in an active state. In contrast, low luminosity AGN with weak broad lines (e.g., Ho et al. 1997; Greene & Ho 2007; Dong et al. 2012) will not be included in the reverberation mapping sample, causing a mild luminosity bias that can flatten the slope of the M_{BH}–σ_* relation. The expected magnitude of the combined effect on the reverberation-mapped AGN sample is, however, small (see for details Schulze & Wisotzki 2011).

The variability criterion can also lead to a selection effect since AGN luminosity variability is a key requirement for a successful reverberation mapping measurements. As there is an anti-correlation between the variability amplitude and AGN luminosity (Cristiani et al. 1997; Vanden Berk et al. 2004), brighter AGN will be preferentially excluded from reverberation mapping campaigns, introducing a bias against higher mass BHs.

The dominating selection effect for the M_{BH}–σ_* relation of AGN samples is likely the observational ability to measure a reliable σ_* of host galaxies. This is particularly challenging for bright AGNs, where the host galaxy spectrum is swamped by the AGN continuum. Thus, only few reliable σ_* measurements exist for $M_{BH} > 10^8\ M_\odot$, leading to a selection bias in the AGN sample. Indeed, the current reverberation mapped AGN sample is skewed toward lower mass BHs, with an apparent lack of σ_* measurements for high mass BHs, limiting the dynamical range of the AGN sample, compared to the quiescent galaxy sample. The combination of these effects, in particular the preferential exclusion of high mass BHs, will naturally lead to a flattening of the slope of the observed M_{BH}–σ_* relation.

We performed a simple Monte Carlo experiment to test the hypothesis: if the $M_{\rm BH}$ distribution of the quiescent galaxies is limited to the $M_{\rm BH}$ distribution of the AGN sample, would the quiescent galaxy sample show a similar flattened slope? We constructed a large number of Monte Carlo samples, for each using the $M_{\rm BH}$ of the 25 reverberation mapped AGNs. Then for each object we assign a σ_* value of a galaxy, which is randomly chosen from the quiescent galaxy sample within a small $M_{\rm BH}$ bin ($\sim$0.3 dex) around the AGN's $M_{\rm BH}$. Then, we fitted the $M_{\rm BH}$–σ_* relations of the Monte Carlo samples. Based on 1000 Monte Carlo realizations, we find a slope of $\beta = 3.81 \pm 0.48$, consistent with that of the AGN sample, implying that the limited $M_{\rm BH}$ distribution causes the flattening of the $M_{\rm BH}$–σ_* relation. If we revert the same experiment by sampling σ_* from the AGN sample and then assign $M_{\rm BH}$ from a galaxy in the quiescent galaxy sample, we find a slope of $\beta = 5.09 \pm 0.50$, consistent with the quiescent galaxy sample.

We conclude that the AGN sample has a σ_* distribution consistent with the quiescent galaxy σ_* distribution, however, it differs in its $M_{\rm BH}$ distribution. Given the same $M_{\rm BH}$ distribution as the AGN sample, the quiescent galaxy sample would follow the same $M_{\rm BH}$–σ_* relation as the AGN sample. Thus, the difference between their apparent relations can be mainly attributed to sample selection effects. At a given σ_*, dynamical methods and reverberation mapping of AGNs probe different regimes in $M_{\rm BH}$. Some BHs will not be observed with dynamical methods, because their sphere of influence is not resolved. On the other hand, some active galaxies will not enter the sample because of the various selection effects discussed above.

This is also consistent with the results for the fit of the inverse $M_{\rm BH}$–σ_* relation for active and quiescent galaxies, presented by Park et al. (2012a). They fitted the $M_{\rm BH}$–σ_* for both samples, first with the forward regression ($p(M_{\rm BH}|\sigma_*)$) and second with an inverse regression ($p(\sigma_*|M_{\rm BH})$). The inverse regression has also been used by Graham et al. (2011) to derive the $M_{\rm BH}$–σ_* relation of quiescent galaxies in order to avoid selection effects in the $M_{\rm BH}$ distribution. Indeed, the inverse fit is not affected by selection effects in the $M_{\rm BH}$ distribution. It therefore can be a powerful tool to reconstruct the underlying relation, free of selection biases, in particular for active galaxies, as demonstrated by Schulze & Wisotzki (2011). However, contrary to the forward regression, the inverse regression does not directly yield the intrinsic $M_{\rm BH}$–σ_* relation, since it determines the conditional probability $p(\sigma_*|M_{\rm BH})$ of the bivariate distribution of $M_{\rm BH}$ and σ_* along an orthogonal direction, independent of any additional selection effects (Schulze & Wisotzki 2011; A. Schulze & L. Wisotzki, in preparation). Reconstructing the intrinsic relation from it requires the knowledge of the bulge distribution function and the intrinsic scatter in the $M_{\rm BH}$–σ_* relation. The exponential decrease of the bulge distribution function at high σ_* in combination with intrinsic scatter in the $M_{\rm BH}$–σ_* relation will lead to a deviation of the inverse relation from the intrinsic relation toward the high $M_{\rm BH}$ end (Schulze & Wisotzki 2011). This upturn naturally causes a steeper slope when fitted by a single power law, consistent with observations (Graham et al. 2011; Park et al. 2012a). Focusing on the strength of the inverse regression to avoid a selection bias on $M_{\rm BH}$, we note that Park et al. (2012a) reported similar slopes of the $M_{\rm BH}$–σ_* relation for active and quiescent galaxies using the inverse regression, while for the forward regression they found a difference in the slopes. This supports our argument that the sample difference is in the range of $M_{\rm BH}$ at a given σ_*, while the range of σ_* at a given $M_{\rm BH}$ in both samples is similar.

5. CONCLUSIONS

To determine and compare the $M_{\rm BH}$–σ_* relationship, we presented updated samples for quiescent and active galaxies, respectively, by combining our new stellar velocity dispersion measurements and previous measurements from the literature. While the quiescent galaxy sample is based on the compilation of McConnell & Ma (2013), the main update is the addition of new, homogeneously measured stellar velocity dispersions for 28 galaxies, based on the spatially resolved H-band spectra obtained with the Triplespec at the Palomar 5m Hale telescope (Kang et al. 2013). These σ_* measurements were corrected for the contribution of galaxy rotation through calculating luminosity-weighted velocity dispersion. The best-fit $M_{\rm BH}$–σ_* relation of quiescent galaxies shows a slope $\beta = 5.31 \pm 0.33$ and an intrinsic scatter $\epsilon = 0.41 \pm 0.05$.

For the reverberation-mapped AGN sample, we improved σ_* measurements for two objects, including NGC 3227, for which we also measured σ_* after correcting for the rotation effect based on the spatially resolved measurements. By updating σ_* for these 2 AGNs, we compiled a sample of 25 AGNs with reverberation $M_{\rm BH}$ and reliable σ_* measurements (Woo et al. 2010) in order to compare with the quiescent galaxy sample and to determine the virial factor f, which is required for the computation of virial $M_{\rm BH}$. First, we determine the virial factor f by matching the AGN sample to our best fit $M_{\rm BH}$–σ_* relation of the quiescent galaxy sample. Second, we presented a new method to obtain the virial factor f, which is to fit simultaneously the $M_{\rm BH}$–σ_* relation of quiescent and active galaxies. Both methods provided consistent results, with a virial factor of $f = 5.1^{+1.5}_{-1.1}$ and $f = 5.9^{+2.1}_{-1.5}$, respectively.

When we determined the $M_{\rm BH}$–σ_* relationship for the active galaxy sample alone, the slope of the $M_{\rm BH}$–σ_* is shallower ($\beta = 3.48 \pm 0.62$) than that of quiescent galaxies, in agreement with previous studies. However, due to the increase of the slope for the quiescent galaxies presented in this paper and other recent studies (Graham et al. 2011; Park et al. 2012a; McConnell & Ma 2013), the two slopes now are consistent with each other only on the 2σ level. While the uncertainty in the slope is still large, this could be evidence for different $M_{\rm BH}$–σ_* relations between quiescent and active galaxies. However, this apparent deviation is resolved when we consider selection effects inherent in the observed samples. The reverberation-mapped AGN sample is slightly biased against low luminosity AGN with weak broad emission lines, hence, low mass BHs. However, more important is a bias against luminous AGN, harboring on average high mass BHs. This is due to a variability bias and a selection bias due to σ_* measurement. The former is due to the anti-correlation between variability amplitude and AGN luminosity, while the latter is caused by the observational challenge to measure σ_* in the presence of a bright nuclear point source. This bias in the $M_{\rm BH}$ distribution gives rise to the observed flattening in the slope. Accounting for the different $M_{\rm BH}$ distributions determined by the dynamical method and by the reverberation mapping method, respectively, we find good agreement of the $M_{\rm BH}$–σ_* relations between active and quiescent galaxies. This result assures the use of broad line AGNs as cosmological tools to probe cosmic evolution of the $M_{\rm BH}$–σ_* relation out to high redshift (e.g., Woo et al. 2006, 2008; Merloni et al. 2010; Wang et al. 2010; Bennert et al. 2011). At the same time, it emphasizes

the need to account for sample selection effects in the design and interpretation of these studies.

We thank the anonymous referee for constructive suggestions. This work was supported by the National Research Foundation of Korea (NRF) grant funded by the Korea government (MEST) (No. 2012-006087). J.H.W acknowledges the support by the Korea Astronomy and Space Science Institute (KASI) grant funded by the Korea government (MEST).

REFERENCES

Barth, A. J., Pancoast, A., Thorman, S. J., et al. 2011, ApJL, 743, L4
Batcheldor, D. 2010, ApJL, 711, L108
Bennert, V. N., Auger, M. W., Treu, T., Woo, J.-H., & Malkan, M. A. 2011, ApJ, 726, 59
Bentz, M. C., Denney, K. D., Cackett, E. M., et al. 2006, ApJ, 651, 775
Bentz, M. C., Peterson, B. M., Pogge, R. W., & Vestergaard, M. 2009, ApJL, 694, L166
Brewer, B. J., Treu, T., Pancoast, A., et al. 2011, ApJL, 733, L33
Cisternas, M., Jahnke, K., Bongiorno, A., et al. 2011, ApJL, 741, L11
Collin, S., Kawaguchi, T., Peterson, B. M., & Vestergaard, M. 2006, A&A, 456, 75
Cristiani, S., Trentini, S., La Franca, F., & Andreani, P. 1997, A&A, 321, 123
Davies, R. I., Thomas, J., Genzel, R., et al. 2006, ApJ, 646, 754
Decarli, R., Falomo, R., Treves, A., et al. 2010, MNRAS, 402, 2453
Denney, K., Bentz, M. C., Peterson, B. M., et al. 2006, ApJ, 653, 152
Denney, K., Peterson, B. M., Pogge, R. W., et al. 2010, ApJ, 721, 715
Dong, X.-B., Ho, L. C., Yuan, W., et al. 2012, ApJ, 755, 167
Fabian, A. C. 1999, MNRAS, 308, L39
Ferrarese, L. 2002, in Current High-Energy Emission Around Black Holes, ed. C.-H. Lee (Singapore: World Scientific Publishing, Co. Pte. Ltd.), 3
Ferrarese, L., & Ford, H. 2005, SSRv, 116, 523
Ferrarese, L., Ford, H., & Jaffe, W. 1996, ApJ, 470, 444
Ferrarese, L., & Merritt, D. 2000, ApJL, 539, L9
Ferrarese, L., Pogge, R. W., Peterson, B. M., et al. 2001, ApJ, 555, L79
Gadotti, D. A., & Kauffmann, G. 2009, MNRAS, 399, 621
Gebhardt, K., Adams, J., Richstone, D., et al. 2011, ApJ, 729, 119
Gebhardt, K., Bender, R., Bower, G., et al. 2000a, ApJL, 539, L13
Gebhardt, K., Kormendy, J., Ho, L. C., et al. 2000b, ApJL, 543, L5
Graham, A. W. 2008, ApJ, 680, 143
Graham, A. W., Onken, C. A., Athanassoula, E., & Combes, F. 2011, MNRAS, 412, 2211
Greene, J. E., & Ho, L. C. 2006, ApJL, 641, L21
Greene, J. E., & Ho, L. C. 2007, ApJ, 670, 92
Greene, J. E., Peng, C. Y., Kim, M., et al. 2010, ApJ, 721, 26
Gültekin, K., Richstone, D. O., Gebhardt, K., et al. 2009, ApJ, 698, 198
Harris, C. E., Bennert, V. N., Auger, M. W., et al. 2012, ApJS, 201, 29
Herrnstein, J. R, Moran, J. M., Greenhill, L. J., & Trotter, A. S. 2005, ApJ, 629, 719
Hicks, E. K. S., & Malkan, M. A. 2008, ApJS, 174, 31
Ho, L. C., Filippenko, A. V., & Sargent, W. L. W. 1997, ApJS, 112, 315
Hu, J. 2008, MNRAS, 386, 2242
Kang, W.-R., Woo, J.-H, Riechers, D., et al. 2013, ApJ, 767, 26
Kaspi, S., Smith, P. S., Netzer, H., et al. 2000, ApJ, 533, 631
King, A. 2003, ApJL, 596, L27
Kormendy, J., Bender, R., & Cornell, M. E. 2011, Natur, 469, 374
Kuo, C. Y., Braatz, J. A., Condon, J. J., et al. 2011, ApJ, 727, 20
Marconi, A., Capetti, A., Axon, D. J., et al. 2001, ApJ, 549, 915
McConnell, N. J., & Ma, C.-P. 2013, ApJ, 764, 184
McConnell, N. J., Ma, C.-P., Gebhardt, K., et al. 2011, Natur, 480, 215
McConnell, N. J., Ma, C.-P., Murphy, J. D., et al. 2012, ApJ, 756, 179
Merloni, A., Bongiorno, A., Bolzonella, M., et al. 2010, ApJ, 708, 137
Morabito, L. K., & Dai, X. 2012, ApJ, 757, 172
Murray, N., Quataert, E., & Thompson, T. A. 2005, ApJ, 618, 569
Nelson, C. H., Green, R. F., Bower, G., Gebhardt, K., & Weistrop, D. 2004, ApJ, 615, 652
Nelson, C. H., & Whittle, M. 1995, ApJS, 99, 67
Netzer, H., Maoz, D., Laor, A., et al. 1990, ApJ, 353, 108
Nowak, N., Thomas, J., Erwin, P., et al. 2010, MNRAS, 403, 646
Onken, C. A., Ferrarese, L., Merritt, D., et al. 2004, ApJ, 615, 645
Onken, C. A., Valluri, M., Peterson, B. M., et al. 2007, ApJ, 670, 105
Pancoast, A., Brewer, B. J., Treu, T., et al. 2012, ApJ, 754, 49
Park, D., Kelly, B. C., Woo, J.-H., & Treu, T. 2012a, ApJS, 203, 6
Park, D. S., Woo, J.-H., Treu, T., et al. 2012b, ApJ, 747, 30
Peng, C. Y., Impey, C. D., Rix, H., et al. 2006, ApJ, 649, 616
Peterson, B. M. 1993, PASP, 105, 247
Peterson, B. M., Ferrarese, L., Gilbert, K. M., et al. 2004, ApJ, 613, 682
Schulze, A., & Gebhardt, K. 2011, ApJ, 729, 21
Schulze, A., & Wisotzki, L. 2011, A&A, 535, A87
Shen, J., & Gebhardt, K. 2010, ApJ, 711, 484
Shen, J., Vanden Berk, D. E., Schneider, D. P., & Hall, P. B. 2008, AJ, 135, 928
Silk, J., & Rees, M. J. 1998, A&A, 331, L1
Tremaine, S., Gebhardt, K., Bender, R., et al. 2002, ApJ, 574, 740
Vanden Berk, D. E., Wilhite, B. C., Kron, R. G., et al. 2004, ApJ, 601, 692
van den Bosch, R. C. E., & de Zeeuw, P. T. 2010, MNRAS, 401, 1770
van den Bosch, R. C. E., Gebhardt, K., Gültekin, K., et al. 2012, Natur, 491, 729
van der Marel, R. P. 1994, MNRAS, 270, 271
van der Marel, R. P., Cretton, N., de Zeeuw, P. T., & Rix, H. 1998, ApJ, 493, 613
Wang, R., Carilli, C. L., Neri, R., et al. 2010, ApJ, 714, 699
Watson, L. C., Martini, P., Dasyra, K. M., et al. 2008, ApJL, 682, L21
Wilson, J. C., Henderson, C. P., Herter, T. L., et al. 2004, Proc. SPIE, 5492, 1295
Woo, J.-H., Treu, T., Barth, A. J., et al. 2010, ApJ, 716, 269
Woo, J.-H., Treu, T., Malkan, M. A., & Blandford, R. D. 2006, ApJ, 645, 900
Woo, J.-H., Treu, T., Malkan, M. A., & Blandford, R. D. 2008, ApJ, 681, 925
Woo, J.-H., Urry, C. M., van der Marel, R. P., Lira, P., & Maza, J. 2005, ApJ, 631, 762
Xiao, T., Barth, A. J., Greene, J. E., et al. 2011, ApJ, 739, 28